The Photogrammetric Record 19(105): 51–66 (March 2004)

MATHEMATICAL MODELLING OF HISTORICAL RECONNAISSANCE CORONA KH-4B IMAGERY

HONG-GYOO SOHN (sohn1@yonsei.ac.kr)

GI-HONG KIM (sfmacho@yonsei.ac.kr)
Yonsei University, Korea

JAE-HONG YOM (jhyom@sejong.ac.kr)
Sejong University, Korea

Abstract

This paper describes three mathematical modelling methods for high-resolution declassified CORONA KH-4B images. Since CORONA images are collected with a panoramic camera, several types of geometric distortions are involved. Two methods use the modified collinearity equations, and the third involves the terrain-dependent rational function model (RFM) which is considered to be a generic sensor model. Comparative analysis of the three mathematical modelling methods is undertaken. The results show that a ± 1·5 pixels level of horizontal and vertical accuracy can be obtained. A digital elevation model (DEM) of a test site is also created.

KEYWORDS: CORONA, KH-4B, DEM

INTRODUCTION

HIGH QUALITY SATELLITE IMAGERY from the Landsat programme has been available to the public since 1972. Until recently, however, only airborne imagery has been available for the era preceding the Landsat programme as a source of high-resolution and broad-scale coverage. More extensive coverage at higher resolution has become available through the declassification of early satellite reconnaissance photography.

CORONA is the programme name for the first operational space reconnaissance project implemented during the cold war era. During its operational phase (1960–1972), panchromatic images of large areas of the world were recorded on film. ARGON and LANYARD were the other two programme names for space imaging capabilities of the 1960s. ARGON, a mapping system that was developed in parallel with CORONA, flew 12 missions between 1961 and 1964. The LANYARD project was designed to gather significant information on suspected antiballistic missile sites near Leningrad. Although LANYARD was expected to be a source of 0·6 m resolution intelligence imagery, it collected a best resolution of only 1·8 m. Because of this, its single mission was considered to be only partially successful. These satellite images were declassified in 1995 and have been available to the public since then (McDonald, 1995).

ARGON imagery has been widely used for environmental studies, since it provides a key opportunity to observe long-term changes in the environment over an extensive area (Sohn et al., 1998; Kim et al., 2001). KH-5, a single panchromatic frame camera system, was used in the ARGON missions. The ground resolution was about 140 m and the ground swath was 540 km × 540 km. To use the images from these missions for specific purposes, each photograph has to be orthorectified. Individual geometric modelling of ARGON photographs has been carried out successfully using bundle adjustments, taking into consideration earth curvature (Sohn and Kim, 2000). Several blocks of ARGON photographs have been successfully orthorectified over Greenland by the self-calibration block bundle adjustment model (Zhou et al., 2002). The frame camera system of the ARGON photographs makes it possible to apply a traditional frame-type aerial photogrammetric approach with only slight modifications.

The CORONA project was originally developed for intelligence and this makes it difficult to model its camera system geometrically for mapping purposes. The KH-4B is a dual panoramic camera system that was mounted on the satellite during the later years of CORONA missions and offered the best ground resolution of about 1·8 m in nadir. Because of this very high ground resolution, CORONA imagery has been recently used for a number of purposes. CORONA, ARGON, and Landsat imagery was used to assess 30 years of land resource changes in west-central Senegal (Tappan et al., 2000). ARGON and Landsat images were geometrically corrected using control points from 1:200 000 scale topographic maps of Senegal. In this study, CORONA imagery was used only for purposes of interpretation and significant geometric distortions were not corrected.

No serious effort to model the camera used for the CORONA imagery accurately and rigorously for mapping purposes has been reported, despite the fact that this is necessary in several application fields. Altmaier and Kany (2002) used the commercial software ERDAS IMAGINE OrthoBASE Pro to generate a digital elevation model (DEM) of a test site from CORONA imagery, but their efforts did not include the application of a mathematical algorithm for removing panoramic deformation, because the procedure is very complicated and the aim of their study was to minimise financial and time demands.

Since CORONA images are collected with a panoramic camera, several types of geometric distortions are involved, and these distortions are maximised toward each end of the photograph. Traditional photogrammetric methods would not be applicable for such imagery. Worst of all, there is no calibration data (fiducial coordinates, lens distortion coefficients, principal point coordinates) or ancillary data (position, velocity vectors, attitude angle) available for CORONA photographs. This may have only minor implications in some fields but will cause serious problems if one wishes to use the images for mapping purposes, or for retrieving geographical information where geo-location accuracy is important. A technique for utilising this data using standard remote sensing software has not been available until now. In this paper three mathematical modelling methods are introduced that are capable of rigorously resolving the geometric problems associated with CORONA KH-4B imagery. A DEM of the study area was generated using the geometric model derived from this study.

IMAGING GEOMETRY OF CORONA KH-4B IMAGERY

The cameras for the CORONA missions were designated KH-1, KH-2, KH-3, KH-4, KH-4A, and KH-4B. For this study the KH-4B imagery was used (offering the

best ground resolution in the CORONA programmes) from mission 1116 as an example to describe typical CORONA imaging geometry. The KH-4B camera is a dual panoramic camera system with a focal length of 61 cm. The resulting ground resolution of the photographs varies across the scan direction of the film. The best resolution is about 1·8 m in nadir. The ground swath was 217 km × 16 km. The flying height is nominally 145 km with two cameras on a common mount, one pointed 15° aft from the vertical and the other 15° forward (Fig. 1). This configuration provided a 30° convergent angle as the satellite moved along the flight direction.

Panoramic cameras are used to obtain a suitable combination of high-resolution and wide-angle coverage of the terrain from space. Exposure of the film is made by a slit in front of the cylindrical photographic film (Wolf, 1983). Due to its panoramic imaging mode, photographs obtained with the CORONA KH-4B camera system contain several types of image distortions which are not present in the normal metric frame camera, as shown in Fig. 2.

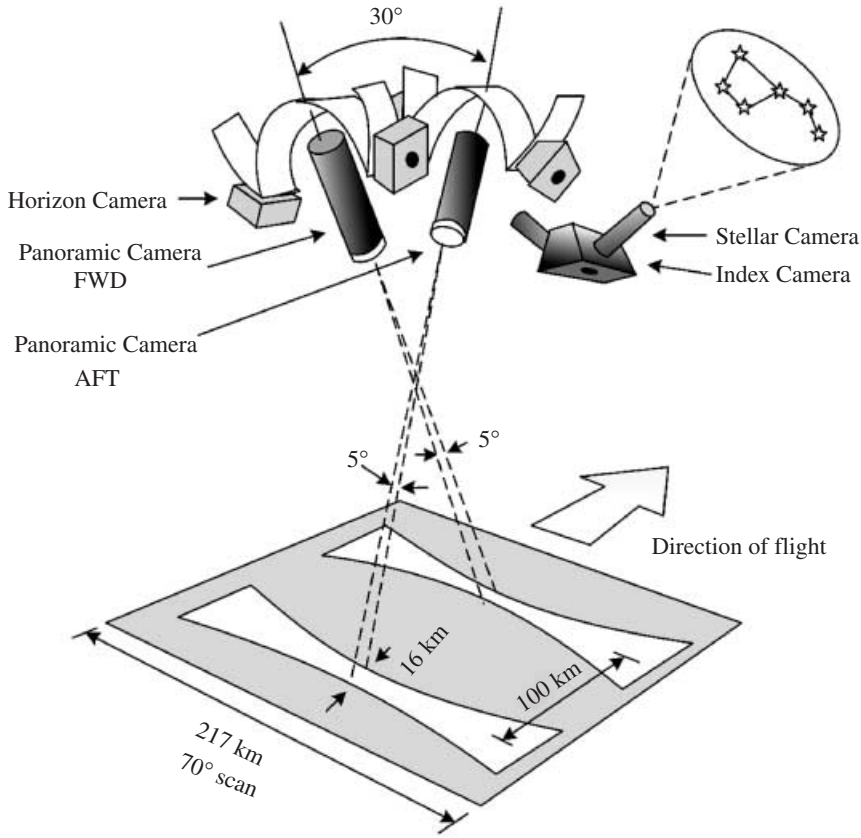

FIG. 1. Imaging geometry of the CORONA KH-4B camera (NRO, 2002).

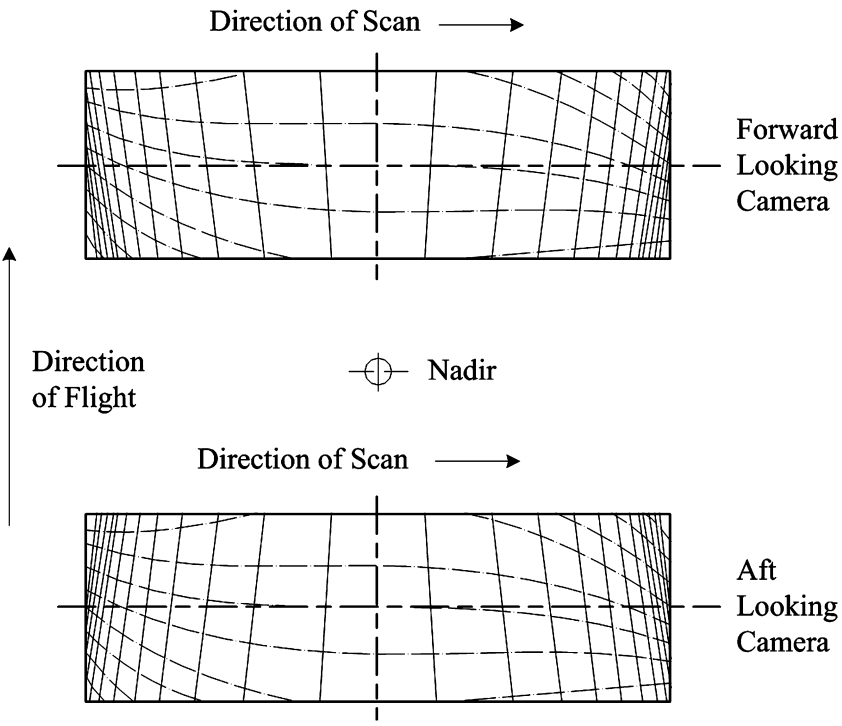

FIG. 2. Schematic diagram of images of a unit grid obtained with a panoramic camera.

RIGOROUS MATHEMATICAL MODELLING FOR CORONA KH-4B IMAGERY

Many types of sensor modelling are based on geometric relationships between image coordinates and object spaces. Their accuracies vary according to the selection of the model solution. Selection of the proper model type is critical, but in most cases the selection is based on convenience and no rigorous evaluation is performed.

To resolve the problem of distortion in CORONA KH-4B imagery three mathematical modelling methods are proposed in this study. First, modified collinearity equations to correct distortions in the image coordinates were implemented. Second, collinearity equations with dynamic exterior orientation parameters modelled as a function of time were also used. Third, a terrain-dependent rational function model (RFM) without a physical sensor model was used.

Definition of Image Coordinate System

Three 2-D image coordinate systems are defined in this study (Fig. 3). One is the image coordinate system (u, v) defined by scanning the CORONA KH-4B film. Its origin is the upper left corner of the scanned image with the u axis in the direction of increasing column numbers and the v axis in the direction of increasing row numbers. Another is the rotated image coordinate system (x_i, y_i) defined by rotating the scanned

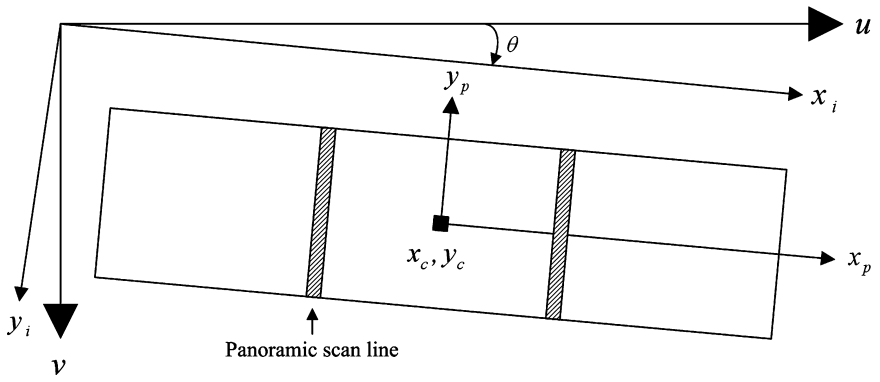

FIG. 3. Definition of image coordinate systems.

image coordinate system by θ using the film edge line located in the upper and lower part of the film. The rotated image coordinates (x_i, y_i) can be calculated by

$$\begin{bmatrix} x_i \\ y_i \end{bmatrix} = \begin{bmatrix} \cos\theta & \sin\theta \\ -\sin\theta & \cos\theta \end{bmatrix} \begin{bmatrix} u \\ v \end{bmatrix}. \tag{1}$$

The third is the panoramic photo coordinate system (x_p, y_p). Its origin is located in the centre of the panoramic film. The centre of the film is not known precisely, due to the lack of a camera calibration file. Its location (x_c, y_c) is placed as an unknown parameter and is called the "pseudo centre" of the panoramic film. The y_p axis is parallel with the y_i axis and with the panoramic scan line of the film recorded at the same exposure time.

The rotated image coordinates (x_i, y_i) are converted into panoramic photo coordinates (x_p, y_p, z_p) by

$$\begin{aligned} x_p &= (x_i - x_c)d \\ y_p &= (y_c - y_i)d \\ z_p &= -f = -609{\cdot}602\,\text{mm}, \end{aligned} \tag{2}$$

where x_c, y_c are the row and column numbers of the pseudo centre, d the image pixel resolution (film scan resolution), and f the focal length. The only available information for focal length is taken from the data book of the National Reconnaissance Office (NRO, 1967) and was maintained as a constant for later photogrammetric procedures.

Method 1: Modified Collinearity Equations (Removing Distortions in Panoramic Photo Coordinates)

The panoramic camera system has a comparatively complicated geometry (Fig. 4). Panoramic photography involves several types of image distortions which are not present in typical frame photography. These distortions differ from those of central-perspective geometry (Slama, 1980), and comprise panoramic distortion, scan

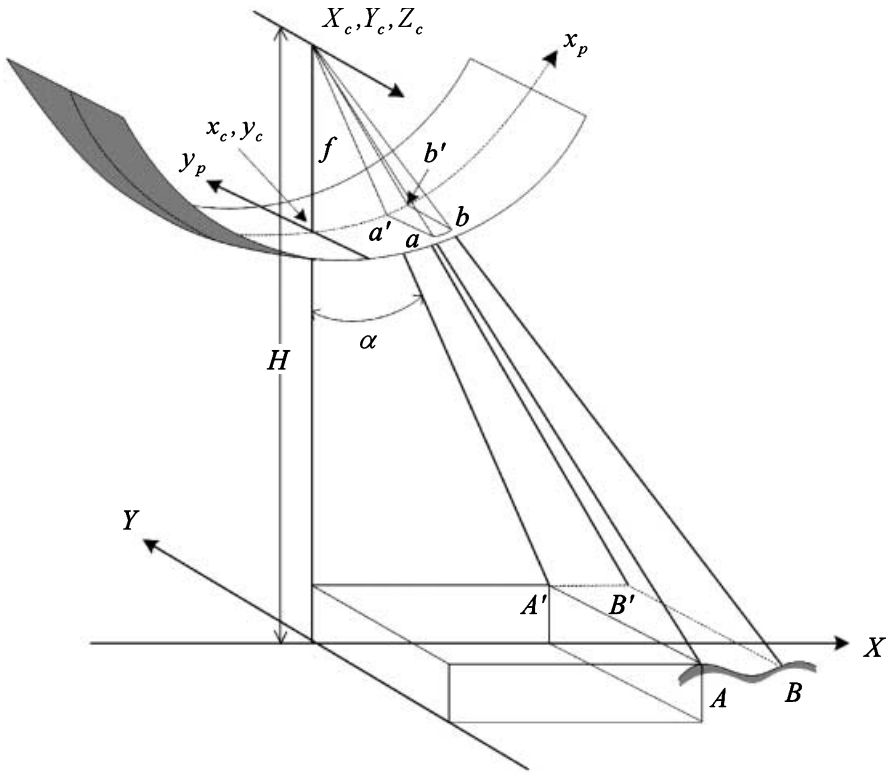

FIG. 4. Isometric view illustrating the geometry of a panoramic image positive.

positional distortion and image motion compensation (IMC) distortion. The regular collinearity equations defined in the frame photo can only be applied after some corrections for these distortions are made.

Panoramic distortion is caused by the cylindrical shape of the film surface and the scanning action of the lens. Assuming that the platform is not moving at the time of exposure, the pertinent geometric relationships between panoramic photo coordinates in cylindrical film and frame photo coordinates in a tangential plane are defined as follows (Fig. 5):

$$x_p = f\alpha \tag{3}$$

$$\alpha = (x_i - x_c)\Delta\alpha \tag{4}$$

$$\Delta\alpha = \frac{d}{f} \tag{5}$$

$$x_f = f \tan\alpha \tag{6}$$

$$y_f = y_p \sec\alpha, \tag{7}$$

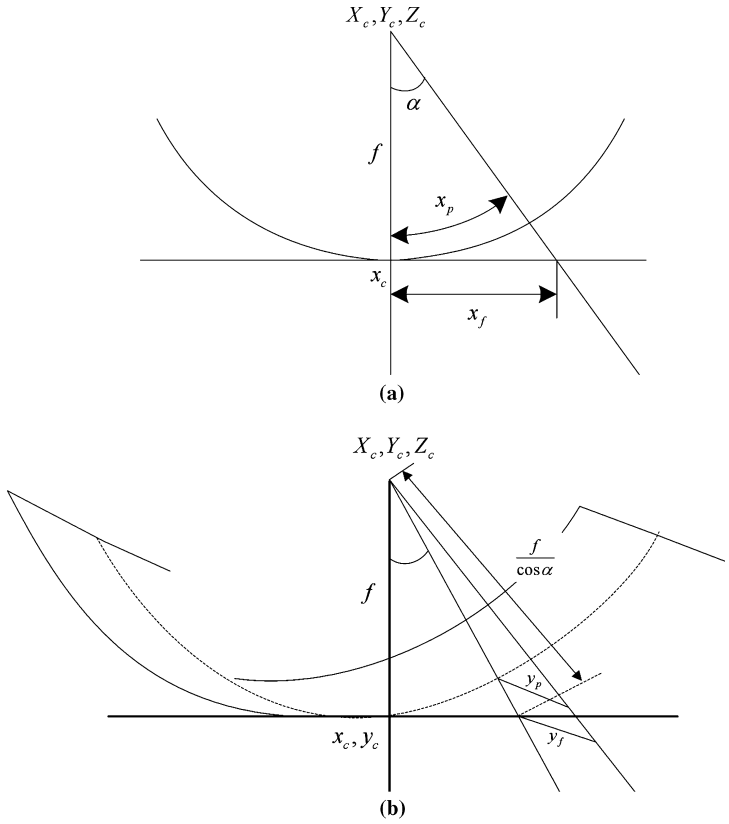

FIG. 5. The relationship of panoramic photo coordinates and frame photo coordinates: (a) relationship between x_p and x_f; (b) relationship between y_p and y_f.

where α is the camera scan angle, $\Delta\alpha$ the scan angle of one pixel (both in radians), and x_f, y_f the frame photo coordinates.

Scan positional distortion is caused by the motion of the platform as the lens scans (Fig. 6(a)). The mathematical relationships are expressed as

$$y_s = \frac{f}{H} V t \cos\alpha \tag{8}$$

$$t = \frac{\alpha}{\delta} \tag{9}$$

$$y_s = \frac{Vf\alpha\cos\alpha}{H\delta}, \tag{10}$$

where y_s is the scan positional distortion component, V the velocity of the platform, t the scan time of the camera, and δ the angular velocity of the camera scan arm.

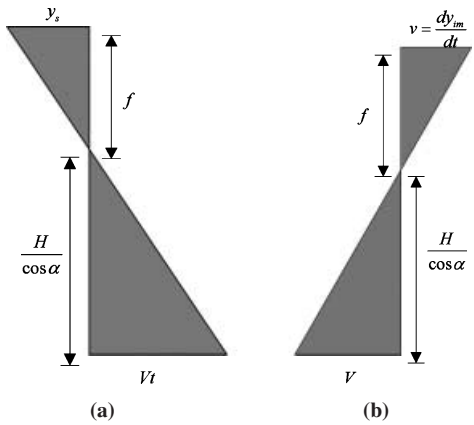

FIG. 6. Geometric relationship of (a) scan positional distortion and (b) IMC distortion.

IMC distortion is caused by the translation of the lens or film surface, which is a motion used to compensate for image motion during exposure time (Fig. 6(b)). The geometry relating to IMC distortion is expressed as

$$v = \frac{dy_{im}}{dt} = \frac{fV\cos\alpha}{H} \tag{11}$$

$$dy_{im} = \frac{fV\cos\alpha\, dt}{H} \tag{12}$$

$$y_{im} = -\frac{fV}{H\delta}\sin\alpha, \tag{13}$$

where y_{im} is the IMC distortion component and v the velocity of the image.

The next step is to relate the coordinates of the panoramic photo coordinate system to those of the frame photo coordinate system. The distortion corrected image coordinates (x'_f, y'_f) are applied to the regular collinearity equations as follows:

$$x'_f = x_f = f\tan\alpha \tag{14}$$

$$y'_f = y_f + (y_s + y_{im})\sec\alpha = \frac{y_p}{\cos\alpha} + \frac{Vf}{H\delta}(\alpha - \tan\alpha) \tag{15}$$

$$\begin{bmatrix} x'_f \\ y'_f \\ -f \end{bmatrix} = s\mathbf{M}\begin{bmatrix} X - X_c \\ Y - Y_c \\ Z - Z_c \end{bmatrix} \tag{16}$$

$$\mathbf{M} = \mathbf{M}_\omega\mathbf{M}_\phi\mathbf{M}_\kappa, \tag{17}$$

where s is the scale factor, $\mathbf{M}$ the rotation matrix in terms of rotation angles (ω, ϕ, κ) between the ground coordinate system and the corrected image coordinate system,

X, Y, Z the ground coordinates, and X_c, Y_c, Z_c the coordinates of the perspective centre. In equation (16), there are nine unknown parameters, which are x_c, y_c, $X_c, Y_c, Z_c, \omega, \phi, \kappa$, and the multiplicative effect of V, H, δ. The unknown parameters are determined by using a minimum of five ground control points (GCPs).

Method 2: Modified Collinearity Equations (Time-dependent Exterior Orientation Parameters)

As the platform moves, the scanning action of the lens projects the terrain onto the cylindrical film. The panoramic scan line of the film is recorded at the same exposure time and maintains a central-perspective projection, similar to linear array sensors. For this, exterior orientation parameters of KH-4B imagery were modelled using time-dependent variables. Since the modelling method involves a considerable number of time-dependent parameters, some simplification was done. Due to high-speed and low-altitude flights and the short scanning time (about 0·5 s), the exterior orientation parameters are modelled as linear functions of time. The collinearity equations are modified to satisfy the CORONA KH-4B imaging geometry accordingly:

$$\begin{bmatrix} 0 \\ y_p + \mathrm{IMC}_t \\ -f \end{bmatrix} = s\mathbf{M}_\alpha\mathbf{M} \begin{bmatrix} X - X_c \\ Y - Y_c \\ Z - Z_c \end{bmatrix} \tag{18}$$

$$\mathbf{M}_\alpha^t \begin{bmatrix} 0 \\ y_p + \mathrm{IMC}_t \\ -f \end{bmatrix} = s\mathbf{M} \begin{bmatrix} X - X_c \\ Y - Y_c \\ Z - Z_c \end{bmatrix} \tag{19}$$

$$\begin{bmatrix} f \sin\alpha \\ y_p + \mathrm{IMC}_t \\ -f \cos\alpha \end{bmatrix} = s\mathbf{M} \begin{bmatrix} X - X_c \\ Y - Y_c \\ Z - Z_c \end{bmatrix}, \tag{20}$$

where $\mathbf{M}_\alpha$ is the rotation matrix of the scan angle at time t.

The corresponding time-dependent exterior orientation parameters are expressed as linear functions:

$$X_c = X_0 + X_1 t$$

$$Y_c = Y_0 + Y_1 t$$

$$Z_c = Z_0 + Z_1 t$$

$$\omega = \omega_0 + \omega_1 t$$

$$\phi = \phi_0 + \phi_1 t$$

$$\kappa = \kappa_0 + \kappa_1 t$$

$$\mathrm{IMC}_t = -\frac{fV}{H\delta}\sin\alpha, \tag{21}$$

where ω, ϕ, κ are the elements of the rotation matrix at time t, and X_c, Y_c, Z_c the ground coordinates of the perspective centre at time t. For any ground point on a line recorded at time t, the corresponding image point should satisfy the collinearity condition when the time-dependent orientation parameters are applied. There are 14 unknown parameters per image, which are $y_c, X_0, X_1, Y_0, Y_1, Z_0, Z_1, \omega_0, \omega_1, \phi_0, \phi_1, \kappa_0, \kappa_1$, and the multiplicative effect of V, H, δ. Through the least squares adjustment using a minimum of seven GCPs the time-dependent orientation parameters can be determined.

Method 3: Terrain-dependent Rational Function Model

The RFM is an alternative sensor model that allows users to perform photogrammetric procedures. This has been considered by the OpenGIS Consortium (OGC, 1999) as a part of the standard image transfer format due to its sensor-independent characteristics. In the case of RFM, the image pixel coordinates are expressed as the ratios of polynomials of object point coordinates. For the ground-to-image transformation, the defined ratio of polynomials is in the form of

$$r = \frac{p_1(X,Y,Z)}{p_2(X,Y,Z)}, \quad c = \frac{p_3(X,Y,Z)}{p_4(X,Y,Z)}, \tag{22}$$

where r and c are the normalised row and column index of pixels in the image and X, Y, and Z are the normalised coordinates of the object space. The general forms of the polynomials used are described as follows:

$$p = \sum_{i=0}^{m_1}\sum_{j=0}^{m_2}\sum_{k=0}^{m_3} a_{ijk}X^iY^jZ^k, \tag{23}$$

where a_{ijk} are polynomial coefficients called rational function coefficients (RFCs).

Without a physical sensor model, the 3D object grid cannot be generated. Therefore, the GCPs on the terrain surface need to be collected in a conventional manner in order to solve the equations for the RFCs (Tao and Hu, 2001). The terrain-dependent RFM is very sensitive to the number and distribution of GCPs. If the distribution of the GCPs is not good, the result cannot be expected to be satisfactory. In addition, the RFM solution is not numerically stable.

Since it was difficult to acquire sufficient GCPs from the old satellite images, the application was restricted to second-order polynomials. Therefore, there are 38 unknown RFCs to solve using a minimum of 19 GCPs.

EXPERIMENTAL RESULTS AND EVALUATION

The two CORONA KH-4B images were acquired on 17th March 1970 (Fig. 7). Films were scanned at 7 μm resolution using the Z/I PhotoScan. The scanner is a high-resolution flatbed scanning system. The corresponding ground pixel size of the test

FIG. 7. Stereopairs of CORONA KH-4B films.

area is about 2·7 m. Land covers about 40% of the image on the right and all the other portions are covered by ocean. The extracted land area is metropolitan Seoul, the capital of the Republic of Korea, and covers approximately 33 km × 17 km.

Fifty-six GCPs were obtained from 1:1000 scale digital topographic maps compiled photogrammetrically from 1:5000 scale aerial photographs. The overall accuracies of the digital topographic map are about 0·7 m horizontally and 0·5 m vertically. The points that were not used for the solution served as check points (Fig. 8). The study area has been rapidly urbanised during the past 30 years, and the roads and buildings have changed substantially. Measuring the GCPs was a time-consuming and labour-intensive task. Some old public buildings such as an elementary school provided reliable positional information.

Since the imagery covers an extensive area, procedures for removing the effect of earth curvature had to be considered. To alleviate the influence of earth curvature, the acquired ground points were transformed into a geocentric coordinate system. Mathematical modelling methods based on the collinearity equations were performed on the geocentric coordinate system. The final results were represented in the map coordinate system after mathematical processing was done in the geocentric coordinate system.

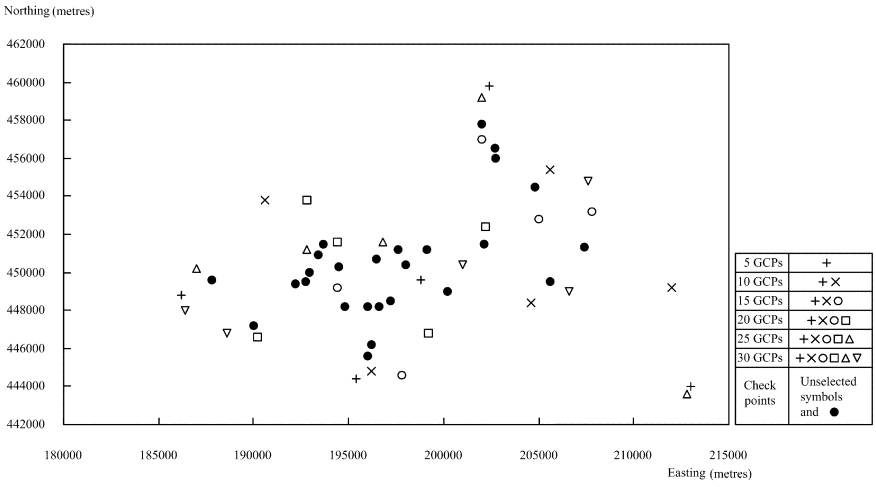

FIG. 8. The distribution of GCPs used and check points.

Accuracy of Triangulation in Stereo Images

The first method, using modified collinearity equations (removing distortions in image coordinates), was applied to stereoscopic CORONA KH-4B images. Uniformly distributed points in the stereomodel were selected as control points out of 56 acquired points and the others were used as check points. To determine the influences of using different numbers of control points, seven different cases ranging from 5 to 30 GCPs were tested. As shown in Table I, the results show that as the number of GCPs increases, the horizontal and vertical root mean square errors (rmse) of the check points decrease. After using 15 GCPs, the positional accuracies of the check points became stable. The accuracy in the Y direction was better than in the X direction. It is speculated that the light rays in stereo images had a high convergence angle in the Y direction, compared with the X direction.

In the second method modified collinearity equations (using time-dependent exterior orientation parameters) were then applied to the study area. Table II shows that the best results are achieved with an rmse in the level of 3·1 m in X, 2·3 m in Y, and 4·0 m in Z, respectively. The accuracy of method 2 was better than that of method 1 with a smaller number of GCPs, but no significant differences between method 1 and method 2 were found with over 15 GCPs. Some 15–20 control points were found to be optimal for the adjustment.

Third, the terrain-dependent RFM without a physical sensor model was applied. The case where $p_2 = p_4 = 1$ worked better than the cases where $p_2 = p_4$ and $p_2 \neq p_4$. The triangulation accuracies of the check points are summarised in Table III. In some tests, it was clear that when GCPs in a high terrain relief were not selected, triangulation accuracies of some check points near them were greatly decreased by over 20 m. It should be noted that when using terrain-dependent RFM the distribution

TABLE I. Triangulation quality in method 1.

Number of control points	*Number of check points*	*Rmse of check points X (m)*	*Rmse of check points Y (m)*	*Rmse of check points Z (m)*
5	51	3·26	2·28	7·04
7	49	4·33	2·10	6·98
10	46	3·64	2·09	4·76
15	41	2·87	1·97	4·45
20	36	2·97	1·97	4·36
25	31	2·96	2·08	4·10
30	26	3·12	2·03	4·31

TABLE II. Triangulation quality in method 2.

Number of control points	*Number of check points*	*Rmse of check points X (m)*	*Rmse of check points Y (m)*	*Rmse of check points Z (m)*
7	49	3·75	2·08	4·70
10	46	3·49	2·11	4·42
15	41	3·03	2·05	4·37
20	36	3·05	2·14	4·23
25	31	3·09	2·27	3·95
30	26	3·16	2·16	4·18

TABLE III. Triangulation quality in method 3.

Number of control points	*Number of check points*	*Rmse of check points X (m)*	*Rmse of check points Y (m)*	*Rmse of check points Z (m)*
20	36	4·93	2·44	6·67
25	31	4·22	2·85	3·98
30	26	3·40	2·45	4·32

of GCPs must be fully considered in advance. If the number and distribution of GCPs are not sufficiently guaranteed, the accuracy is unreliable.

Generation of DEM

Using the modified collinearity equations (method 1), a 10 m grid interval DEM was generated from the stereoscopic CORONA KH-4B images. The convergent angle is about 30°, and the base/height ratio of the model was approximately 0·59. The panoramic scan angles of the study area in both images are about 26° in the east direction. The reason for choosing method 1 to generate the DEM is that the modelling accuracy is stable and standard remote sensing or photogrammetric software can be used. The coordinates on the panoramic CORONA KH-4B image were transformed to the equivalent of a frame photo and generated resampled frame photo images. The exterior orientation and unknown parameters were calculated from 20 GCPs used in the previous study.

A DEM was generated using the OrthoBASE module of ERDAS IMAGINE. To assess the quality of the DEM generated from the CORONA imagery, it was compared with a DEM generated from the contours of a 1:1000 scale digital topographic map. The selected area covers the central part of Seoul where Mt. Namsan is located. The approximate coverage area is 2·65 km × 1·67 km with an elevation ranging from 19 m to 271 m. The results of the comparison are summarised in Table IV.

The rmse for a total of 44 255 grid points is ± 5·81 m. The large difference areas are concentrated on the north-eastern part of Mt. Namsan since this part is poorly illuminated. The extraction of topographic contours from each DEM at the 20 m interval provided a visual comparison of the two DEMs (Fig. 9). Considering the 2·7 m ground resolution of the CORONA imagery, this is a reasonable result over a mixed urban and mountain area.

TABLE IV. Statistical comparison of the two DEMs.

	DEM elevations from 1:1000 digital topographic maps for check points	*DEM elevations from CORONA KH-4B images*	*Differences*
Number of points	44 255	44 255	44 255
Mean (m)	99·91	101·47	3·96 (mean error)
Standard deviation (m)	56·17	57·60	5·60
Maximum (m)	270·81	276·18	36·36
Minimum (m)	18·96	10·13	−32·96
Rmse (m)	–	–	5·81

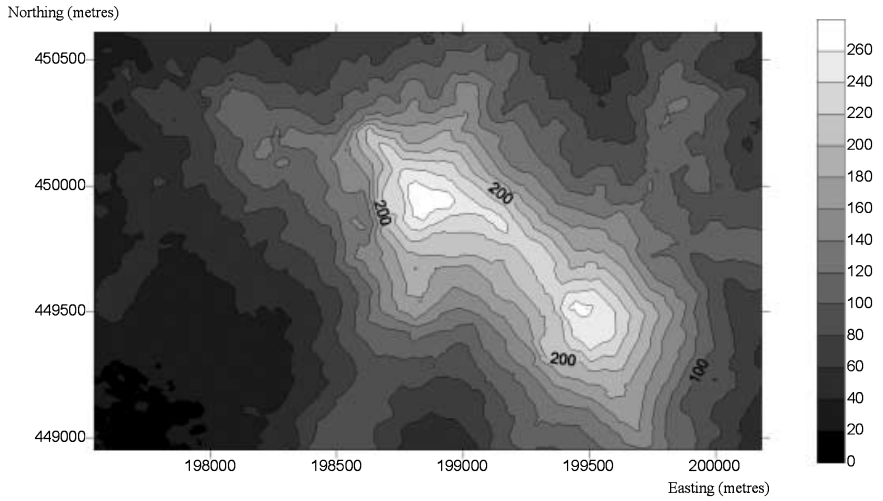

(a)

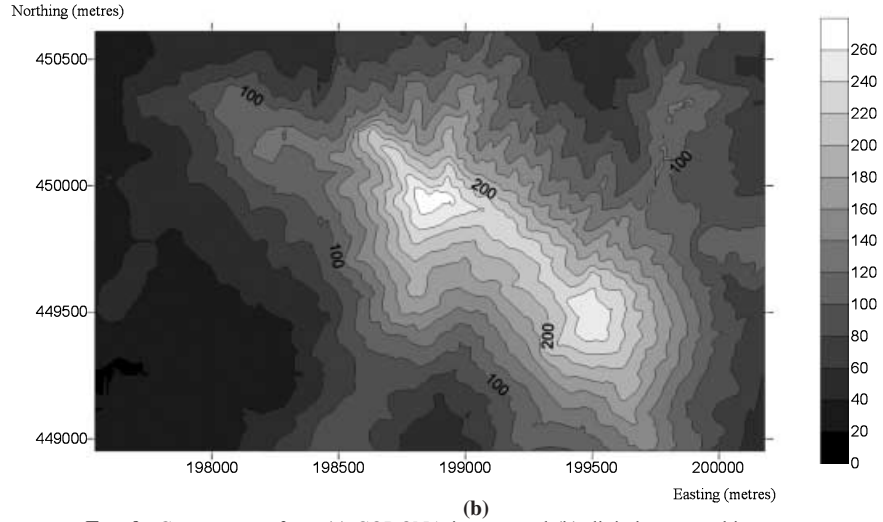

(b)

FIG. 9. Contour map from (a) CORONA images and (b) digital topographic map.

CONCLUSIONS

Three mathematical modelling methods were successfully applied to "old era" CORONA KH-4B images. In method 1, image domain corrections effectively remove distortions caused by the panoramic scanning action and the moving platform. In method 2, the panoramic scanning action and the moving platform are modelled as dynamic exterior orientation parameters. Methods 1 and 2 are essentially based on collinearity equations. Method 3 uses the ratio of two polynomial functions.

As a result of using the mathematical modelling methods described in this paper, a ± 1·5 pixels level of horizontal and vertical accuracy was obtained, which is equivalent to ± 4 m on the ground, with over 15 GCPs using methods 1 and 2. The triangulation accuracy of terrain-dependent RFM was poorer than the methods based on the collinearity equations. Since measuring GCPs is a very difficult task in ''old era'' images, RFM is considered to be unsuitable for precise applications due to its high dependency on the number and distribution of GCPs. Since the panoramic image coordinates can be transformed into the frame photo coordinates, method 1 is attractive for regular users and is readily applicable to existing photogrammetric software with fixed exterior orientation parameters.

This paper also demonstrated that CORONA KH-4B images could be used to produce DEMs. The data from high-resolution CORONA imagery can provide useful information for various analyses which involve the processing of image data obtained prior to the 1970s. Especially in change detection applications, thematic maps and land use classification maps can be produced using CORONA imagery and the mathematical modelling methods introduced in this paper.

Acknowledgements

The authors would like to thank anonymous reviewers for the time and effort spent on improving the contents of the paper. This work was supported by grant No. R01-2000-000-00371-0 from the Basic Research Program of the Korea Science & Engineering Foundation.

References

Altmaier, A. and Kany, C., 2002. Digital surface model generation from CORONA satellite images. *ISPRS Journal of Photogrammetry & Remote Sensing*, 56(4): 221–235.

Kim, K. T., Jezek, K. C. and Sohn, H. G., 2001. Ice shelf advance and retreat rates along the coast of Queen Maud Land, Antarctica. *Journal of Geophysical Research*, 106(C4): 7097–7106.

McDonald, R. A., 1995. Corona: success for space reconnaissance, a look into the cold war, and a revolution for intelligence. *Photogrammetric Engineering & Remote Sensing*, 61(6): 689–720.

NRO (National Reconnaissance Office), 1967. *The KH-4B Camera System*. 3 pages.

NRO (National Reconnaissance Office), 2002. http://www.nro.gov/index5.html [Accessed: 1st February 2003].

OGC (OpenGIS Consortium), 1999. The OpenGIS Abstract Specification-Topic 7: Earth Imagery. http://www.opengis.org/techno/abstract/99-107.pdf [Accessed: 1st February 2003].

Slama, C. C. (Ed.), 1980. Panoramic cameras. In *Manual of Photogrammetry*. Fourth edition. American Society of Photogrammetry, Falls Church, Virginia. 1056 pages. Section 4.2.2: 196–207.

Sohn, H. G., Jezek, K. C. and van der Veen, C. J., 1998. Jakobshavn Glacier, West Greenland: 30 years of spaceborne observations. *Geophysical Research Letters*, 25(14): 2699–2702.

Sohn, H. G. and Kim, K. T., 2000. Horizontal accuracy assessment of ARGON imagery. *Journal of Korean Society of Civil Engineers*, 4(1): 59–65.

Tao, C. V. and Hu, Y., 2001. A comprehensive study of the rational function model for photogrammetric processing. *Photogrammetric Engineering & Remote Sensing*, 67(12): 1347–1357.

Tappan, G. G., Hadj, A., Wood, E. C. and Lietzow, R. W., 2000. Use of Argon, Corona, and Landsat imagery to assess 30 years of land resource changes in West-Central Senegal. *Ibid.*, 66(6): 727–735.

Wolf, P. R., 1983. *Elements of Photogrammetry*. Second edition. McGraw-Hill, New York. 628 pages.

Zhou, G., Jezek, K., Wright, W., Rand, J. and Granger, J., 2002. Orthorectification of 1960s satellite photographs covering Greenland. *IEEE Transactions on Geoscience and Remote Sensing*, 40(6): 1247–1259.

Résumé

On présente dans cet article trois méthodes de modélisation mathématique pour des images à haute résolution CORONA KH-4B déclassifiées. Etant donné que les images CORONA sont saisies à l'aide d'une caméra panoramique, il s'ensuit que plusieurs types de distorsions géométriques sont impliqués.

Deux méthodes recourent aux équations de colinéarité modifiées tandis que la troisième met en œuvre le modèle à fonction rationnelle dépendant du terrain (RFM), que l'on considère comme un modèle propre au capteur. Les auteurs ont analysé comparativement les trois méthodes de modélisation mathématique. Les résultats montrent que l'on peut obtenir des niveaux de précision horizontale et verticale de ±1,5 pixel. Les auteurs ont également réalisé un modèle numérique des altitudes (MNA) sur un site témoin.

Zusammenfassung

Dieser Beitrag beschreibt drei Methoden zur mathematischen Modellierung von jetzt freigegebenen hochauflösenden CORONA KH-4B Bilddaten. Da CORONA Bilder mit einer panoramischen Kamera aufgenommen werden, treten mehrere Arten von geometrischen Verzerrungen auf. Zwei der beschriebenen Modellierungsmethoden nützen modifizierte Kollinearitätsgleichungen und die dritte Methode verwendet ein geländeabhängiges Modell mit Rationalen Funktionen (RFM), das als generischen Sensormodell betrachtet werden kann. Die Autoren stellen vergleichende Analysen aller drei mathematischen Methoden vor. Die Ergebnisse zeigen, dass Genauigkeiten von ±1·5 Pixel in Lage- und Höhe erreicht werden können. Die Autoren präsentieren weiterhin ein generiertes Digitales Höhenmodell (DEM) des Testgebietes.

Resumen

Este artículo describe tres métodos de modelado matemático para imágenes de alta resolución CORONA KH-4B que han sido liberadas de su clasificación como material restringido. Las imágenes CORONA se captan con una cámara panorámica lo que resulta en la aparición de varios tipos de distorsiones geométricas. Se presentan dos métodos de modelado que usan las ecuaciones de colinealidad modificadas, y un tercero basado el Modelo de Funciones Racionales (MFR) dependiente del terreno y que está considerado como un modelo genérico de sensores. Los autores presentan un análisis comparativo de los tres métodos de modelado matemático. Los resultados muestran que se puede obtener un nivel de exactitud horizontal y vertical de ±1.5 píxel. Los autores además calculan un Modelo Digital del Terreno (MDT) de una zona de ensayo.

